Functional and Developmental Impact of Cytosolic Protein N-Terminal Methionine Excision in Arabidopsis[1[w]]

Simon Ross[2], Carmela Giglione*, Michèle Pierre, Christelle Espagne, and Thierry Meinnel

Protein Maturation Group, Institut des Sciences du Végétal, Unité Propre de Recherche 2355, Centre National de la Recherche Scientifique, F–91198 Gif-sur-Yvette cedex, France

Protein N-terminal methionine (Met) excision (NME) is carried out by two types of Met aminopeptidases (MAPs), MAP1 and MAP2, in eukaryotes. Three enzymes, MAP1A, MAP2A, and MAP2B, have been identified in the cytoplasm of Arabidopsis (*Arabidopsis thaliana*). MAP transcript quantification revealed a predominance of *MAP2B* and developmental and organ-specific regulation of both *MAP1A* and *MAP2*s. By combining reverse genetics and reverse chemogenomics in transgenic plant lines, we have devised specific and reversible switches for the investigation of the role of cytoplasmic NME in Arabidopsis and of the respective contributions of the two types of cytoplasmic MAPs throughout development. dsRNA interference and knockout (KO) plant lines targeting either MAP1A alone or both MAP2s simultaneously were constructed and shown to display wild-type phenotypes. In the *MAP1A* KO context, modulating MAP2 activity by treatment with various concentrations of the specific drug fumagillin impaired plant development, with particularly strong effects on the root system. Reciprocally, complete MAP2 inhibition in various *MAP1A* knocked-down genetic backgrounds also generated a gradient of developmentally abnormal plants, but the effects on the root system were milder than in the KO context. In the absence of MAP2 activity, the severity of the phenotype in the *MAP1A* knocked-down lines was correlated to the extent of *MAP1A* mRNA accumulation. Complete cytoplasmic NME inactivation blocked development after plant germination. Thus, in plants, (1) cytoplasmic NME is essential; (2) MAP1A and MAP2s are functionally interchangeable, which is not the case in fungi and animals, as a complete block of either MAP-type activity does not cause any visible molecular or phenotypic effect; and (3) a minimal level of cytoplasmic MAP is required for normal development.

In living organisms, whatever the cell compartment, proteins are always synthesized with Met as the first residue even if a nonconventional initiation codon (i.e. non-AUG) is used (for review and references, see Giglione and Meinnel, 2001; Giglione et al., 2004). However, this first Met is specifically removed from most mature proteins (Meinnel et al., 1993; Bradshaw et al., 1998; Giglione and Meinnel, 2001). In the course of protein N-terminal Met excision (NME), the free amino-terminal Met is removed by Met aminopeptidase (MAP) cleavage. Unlike eubacteria, which possess only one type of MAP (MAP1), eukaryotes possess a second type of MAP, MAP2, which has similar substrate specificity to MAP1 (Kendall and Bradshaw, 1992; Chen et al., 2002). MAP2s and MAP1s play identical enzymatic roles and have very similar three-dimensional (3D) structures, but their amino acid sequences differ considerably. In contrast, levels of sequence identity are high for MAPs of the same type (Lowther and Matthews, 2002; Giglione et al., 2004). The recent discovery that cytoplasmic MAP2s are the specific cellular target of natural compounds like fumagillin, acting as antiangiogenic, antitumoral, or immunosuppressive agents, has revived interest in NME (Ingber et al., 1990; Griffith et al., 1997, 1998; Sin et al., 1997; Turk et al., 1999; Towbin et al., 2003). Several of these compounds have also been shown to have antiproliferative effects in unicellular eukaryotes, such as ameba (Killough et al., 1952), microsporidians (Weiss et al., 2001), trypanosomatida, and apicomplexa (Zhang et al., 2002), all of which cause severe parasitic diseases in humans. Significant progress has recently been made in the characterization of this process in higher eukaryotes (for review, see Giglione et al., 2004). NME has been shown to occur in all compartments in which de novo protein synthesis occurs: the cytoplasm, mitochondria, and plastids. Experimental data have shown that MAP1s are found in both the organelles and the cytoplasm (MAP1As) of all higher eukaryotes, including mammals and plants (Giglione et al., 2000; Serero et al., 2003). Unlike MAP1s, MAP2s are found specifically in the cytoplasm (Giglione et al., 2004). In higher plants, various organelle-targeted MAPs (MAP1B, MAP1C, and MAP1D; Giglione et al.,

[1] This work was supported by the Centre National de la Recherche Scientifique (grant no. PGP04–11; Poste de Chercheur Associé grant to S.R.), by Fonds National de la Science (grant no. BCMS275), and by the Association pour la Recherche sur le Cancer (grant no. 3363).

[2] Present address: Unité de Pathologie Végétale, Institut National de la Recherche Agronomique, Route de St. Cyr, F–78026 Versailles cedex, France.

* Corresponding author; e-mail giglione@isv.cnrs-gif.fr; fax 33–1–69–82–36–07.

[w] The online version of this article contains Web-only data.

Article, publication date, and citation information can be found at www.plantphysiol.org/cgi/doi/10.1104/pp.104.056861.

2004) and three cytosolic MAPs (MAP1A, MAP2A, and MAP2B) have been characterized as members of the NME machinery (Giglione et al., 2000). The cytoplasmic NME machinery in animals and plants displays the same specificity because proteins having their N-terminal Met removed with the MAP cleavage rule (Meinnel et al., 1993) were identified in each reign (perform at http://www.expasy.org/srs5/ query ''FtKey = INIT_MET'' and combine with query ''Organism = Arabidopsis for instance'').

Various studies involving attempts to inactivate *MAP* genes have shown that NME is an essential process in bacteria (for review, see Giglione et al., 2004). NME is also essential in the yeast *Saccharomyces cerevisiae*, as the inactivation of both the *MAP*1 and *MAP2* genes is lethal (Li and Chang, 1995). However, *MAP*1 inactivation alone results in a large decrease in growth rate, which is indicative of the dominant role of *MAP*1 in fungal NME (Chang et al., 1992; Dummitt et al., 2003). In animals, MAP2s, also known as p67, behave as bifunctional proteins. Their N-terminal domain maintains the translation initiation factor eIF2 in a fully active form by protecting its α-subunit from phosphorylation (Ray et al., 1992). This so-called protection of eIF2α phosphorylation (POEP) activity is mediated by the N-terminal Lys-rich domain I and is independent of NME activity. The down-regulation of MAP2 leads to the phosphorylation of eIF2α, resulting in the inhibition of protein synthesis, which ultimately triggers apoptosis (for review, see Datta, 2000). The C-terminal domain of animal MAP2s displays NME activity (Liu et al., 1998; Yang et al., 2001). Natural compounds like fumagillin do not impair the interaction of MAP2 with eIF2α, but completely inhibit NME activity. As animal MAP2 has both NME and POEP activity, any change in the concentration of this enzyme in the cell is likely to reduce both activities. This seems to be the case in *Drosophila melanogaster*, in which *MAP2* gene inactivation has been shown to impair tissue growth and lead to early embryo death (Cutforth and Gaul, 1999). Clearly, functional studies in which the production of MAP2 is not affected are required to determine the impact of cytoplasmic NME in these eukaryotes, as decreasing the amount of MAP2 is also likely to decrease POEP activity. Plant and fungal MAP2s do not have the POEP domain (Giglione et al., 2000) and are therefore unlikely to display POEP activity. This hypothesis is supported by the observation that yeast *MAP2* knockout (KO) mutants are fully viable (Li and Chang, 1995).

As they are unlikely to display a MAP2-dependent POEP effect, plants appear particularly suitable for investigations into the respective contributions of the two types of MAP to cytoplasmic NME in a higher eukaryote by means of reverse genetics-mediated functional strategies. We have already used Arabidopsis (*Arabidopsis thaliana*) as a model to elucidate the role of NME in another cell compartment and the impact of this process on development. Plastid NME, despite the fact that it involves only a few dozen target proteins, has been shown to be essential in plants. The inactivation of plastid NME prevents the immature plastid from developing into a functional chloroplast. This effect results from the strong instability of certain essential plastid-encoded proteins when plastid NME is blocked (Giglione and Meinnel, 2001; Serero et al., 2001; Giglione et al., 2003). In this study, we investigated the impact of NME in the cytoplasm during the development of Arabidopsis. This process involves 55% of the proteome, i.e. more than 15,000 different protein targets (Boisson et al., 2003). Using an integrated array of experimental approaches, we were able to show that (1) cytoplasmic NME is essential for plant development; (2) a minimal level of total cytoplasmic MAP is required for correct plant development; (3) low levels of MAP2 cannot compensate for the absence of or very low levels of MAP1A; and (4) the natural compound fumagillin specifically targets the activity of both MAP2A and MAP2B, but not that of MAP1A in plants, as previously demonstrated in animals and fungi.

RESULTS

Quantification of *MAP* Transcripts Shows the Predominance of *MAP2B* RNA and the Developmental and Organ-Specific Regulation of Both *MAP1A* and *MAP*2s

As observed in other species, Arabidopsis contains two types of cytosolic MAPs, MAP1A and two MAP2s, MAP2A and MAP2B. These are the only cytosolic MAPs isolated (Table I; Giglione et al., 2000). The three corresponding genes are *MAP1A*, *MAP2A*, and *MAP2B*. *MAP2A* and *MAP2B* have identical intron-exon organizations, produce mRNAs of the same size, and their open reading frames are 86% identical overall (Giglione et al., 2000). MAP2A and MAP2B catalytic domains are more than 90% identical. The amino acid sequence of the MAP1A catalytic domain is approximately 50% identical to those of the 3 organellar MAP1s. Low levels of identity occur between MAP1s and MAP2s (Supplemental Fig. 1). The data concerning the MAP protein family from Arabidopsis are summarized in Table I. Except for MAP1A (this article), no specific antibody is yet available for the other MAPs, including both MAP2s.

Few data on cytoplasmic MAP expression and regulation in a whole higher eukaryote are available. We therefore investigated the expression profiles of all three genes in various organs and during plant development by means of real-time PCR experiments. A cytoplasmic *MAP* transcript was present in all tissues and at all developmental stages examined. *MAP2* transcripts accumulated in all organs tested, but the amount depended on the organ considered (Fig. 1A). *MAP2B* transcripts were the most abundant of the two *MAP2*s. *MAP1A* transcripts were observed in all organs tested, except siliques, in which they were undetectable. *MAP1A* transcripts were strongly induced during the early stage of development, beginning at root

Table I. *Various MAP genes and corresponding proteins in Arabidopsis*

Gene Name[a]	TAIR Entry[b]	No. of Open Reading Frame Codons (Size)[c]	Percent Identity with MAP1A[d] (MAP2B/MAP2A)	Cellular Localization of the Protein[a]
MAP2A	At2g44180	440 (49)	<20[d] (100)	Cytoplasm
MAP2B	At3g59990	439 (49)	<19[d] (86)	Cytoplasm
MAP1A	At2g45240	398 (44)	100	Cytoplasm
MAP1B	At3g25740	369 (35)	50	Chloroplast
MAP1C	At1g13270	344 (31)	46	Chloroplast, mitochondrion
MAP1D	At4g37040	350 (33)	48	Chloroplast, mitochondrion

[a]Experimental data are from Giglione et al. (2000). Note the nomenclature used in this article was updated recently (Giglione et al., 2004). [b]TAIR, The Arabidopsis Information Resource (http://arabidopsis.org/). [c]Deduced protein size is expressed in kilodaltons and corresponds to that of the fully processed protein, taking into account NME and signal peptide cleavage as determined at http://www.cbs.dtu.dk/services/TargetP. [d]< indicates that only local identity in the catalytic domain was obtained and that the value indicated corresponds to that of the highest value determined for 10 contiguous amino acids (for an alignment of MAP1 and MAP2, see Supplemental Fig. 1).

emergence on day after imbibition (DAI) 2. Significant levels of induction were also observed for both *MAP2* transcripts until DAI 4 (Fig. 1A).

Strong Decrease in the Level of Expression of the Genes of the Two MAP Groups Reveals No Apparent Phenotype

Functional analysis of cytoplasmic NME in Arabidopsis by insertional reverse genetics is difficult because three genes are involved in the process (Table I) and *MAP2A* (At2g44180) and *MAP1A* (At2g45240) are very close neighbors on chromosome 2, making it difficult to identify double mutants if KO plants were isolated for each gene. To investigate NME by reverse genetics, we used dsRNA interference (RNAi) to construct plant lines with knocked-down (KD) *MAP* expression. First, two RNAi vectors, one targeting *MAP1A* and the other targeting both *MAP2A* and *MAP2B*, were constructed. We selected 50 drug-resistant T_1 plants at random for each construct and followed their development until seed production. All were shown to have the relevant construct target gene-inverted repeats, as shown by PCR analysis, and produce the RNAi transcript, as shown by northern blotting (data not shown). Various *MAP1A* and *MAP2* KD T_1 lines (*Ψmap1A*, *Ψmap2*) were selected with this method. The level of the relevant target *MAP* gene transcript was determined by semiquantitative reverse transcription (RT)-PCR in 10-DAI-old plantlets grown on normal medium (Fig. 1B). *MAP1A*, *MAP2B*, and *MAP2A* transcript levels were compared with those in wild-type plants, and progeny from one of the *ctl* T_1 lines were examined. The plants from each *Ψmap1A* line had much lower levels (8% ± 1% of wild type) of *MAP1A* than wild type (Fig. 1, A and B). However, we also isolated several *Ψmap1A* lines with various, smaller decreases in *MAP1A* transcripts (data not shown). In the *Ψmap2* progeny plant, *MAP2B* and *MAP2A* transcript levels were strongly reduced (7% ± 3% and 29% ± 3% of wild type, respectively). *MAP* transcript levels were unaffected in the progeny of the *ctl* T_1 line. No obvious abnormalities in morphology (growth rate and size) or rate of development (germination time, flowering time, and seed yield) were detected after systematic comparisons with wild-type plants. In line with this, no difference was observed when the protein patterns of plants from several *Ψmap1A* and *Ψmap2* lines were compared with those of the wild-type or *ctl* line (data not shown).

Together, these data strongly suggested that both *MAP* types were functionally interchangeable. To exclude that the small remaining amount of functional MAP1 or MAP2 observed in either RNAi line could be sufficient to allow normal plant development, KO mutants for both *MAP*s were searched. We screened various Arabidopsis T-DNA mutant collections in vitro or in silico for insertions in *MAP1A* and *MAP2* genes. No true KO lines have yet been obtained for *MAP2A*. In the putative *MAP2B*-inserted line, SALK_100162, the T-DNA insertion turned out to have occurred outside the open reading frame, in contrast to the sequence data available. We therefore excluded this line from the analysis. One putative mutant line was identified for *MAP1A* with a T-DNA insertion point within the first intron of the gene (Fig. 2A). Lines homozygous for a T-DNA insertion resulting in *MAP1A* inactivation (*map1A-1*) were obtained and purified. The T-DNA insertion in line *map1A-1* is located downstream of the first Cys codon of the first exon. As this Cys, which is part of the double zinc finger motif that is crucial for in vivo MAP1A activity in yeast (Zuo et al., 1995), line *map1A-1* was expected to correspond to a true *MAP1A* KO mutant. RT-PCR analysis confirmed the absence of any detectable full-length *MAP1A* transcript in line *map1A-1* in contrast to wild type (Fig. 2B). Accordingly, western-blot experiments showed that line *map1A-1* contained no detectable MAP1A and corresponded to a true *MAP1A* inactivation (Fig. 2C). Line *map1A-1* behaved similarly to wild type and displayed no visible mutant phenotype under standard greenhouse growth conditions. We investigated the expression profiles of the *MAP* genes by real-time PCR and noticed that both *MAP2* transcript levels were identical to those of wild type (Fig. 1A). To definitely exclude the occurrence of any subtle differences between line *map1A-1* and wild type, comparison of their two-dimensional gel electrophoresis (2-DE) protein patterns were performed

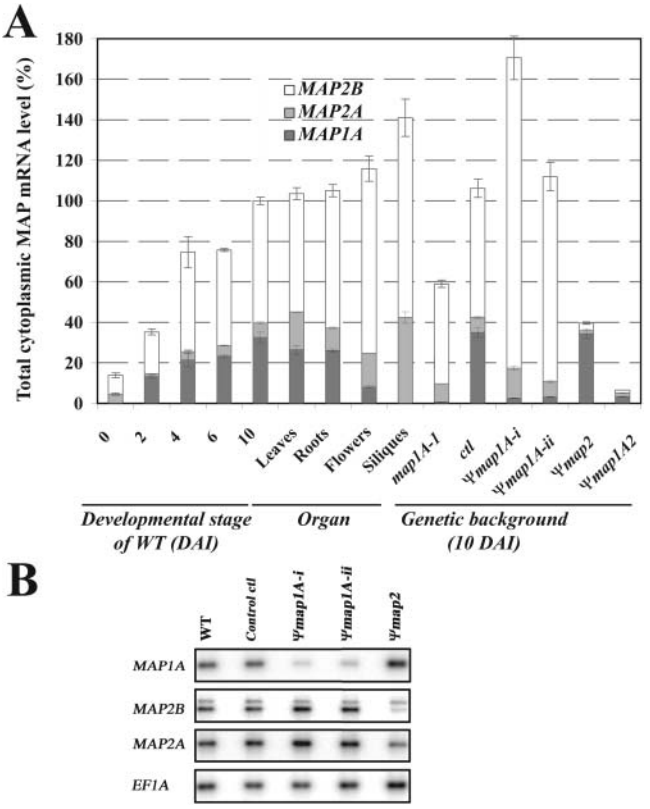

Figure 1. Relative transcript levels for Arabidopsis cytoplasmic MAPs in various organs, during development, and in the RNAi mutants. A, Levels of transcripts for cytoplasmic *MAPs* are expressed relative to *EF1A* transcript levels. Measurements were made by real-time PCR. For comparison with the levels of the various transcripts in the RNAi mutants, the percentage of cytoplasmic MAP levels in wild-type plantlets at 10 DAI was taken as 100%. The SD [$d(x/y)$] corresponding to each x:y (i.e. *MAP:EF1A*) ratio was calculated for each value using the following formula, where $d(x)$ and $d(y)$ correspond to the individual deviation of each x and y measurement, respectively: $d(x/y) = [d(x)^2/y^2 + x^2 \cdot d(y)^2/y^4]^{1/2}$. B, Semiquantitative PCR in various RNAi lines from one representative experiment. The experiment was repeated with new plants and equivalent decreases in MAP levels with respect to controls were observed. All products were of the expected size, with the exception of a minor, high-M_r band resulting from MAP2B PCR; negative controls were at background levels. Additional cycles were performed for MAP2B PCR and the two fragments isolated and sequenced. The predominant lower M_r fragment corresponded to the MAP2B cDNA sequence, the higher M_r band corresponded to the mRNA sequence plus an unspliced intron (nucleotides 90,507–90,742; GenBank AL138647) yielding a truncated, nonfunctional protein.

(Fig. 2D). No qualitative difference on a set of several hundred of the major protein spots was observed by pairwise analysis. This was indicative that line *map1A-1* behaved similarly to wild type, and that the function of MAP1A is compensated by that of MAP2.

Challenging Plant Cytoplasmic NME with L-Met

As no *MAP2* (i.e. MAP2A + MAP2B) KO line is yet available, we investigated the role of plant cytoplasmic NME further using an inhibitor active against cytoplasmic MAPs. Few such inhibitors are known (Giglione et al., 2004). Recently, L-Met, the product of the reaction catalyzed by MAPs, was shown to inhibit both *Homo sapiens* MAPs (HsMAPs), but with different binding constants: 0.15 mM for MAP2 and 5 mM for MAP1A (Dummitt et al., 2003). The 3D structures of the complex of L-Met with MAP1 and MAP2 are available under protein data bank (PDB) entries 1C21 and 1KQ9. These structures show that L-Met binds to conserved residues in the active site of both MAP species (Fig. 3A; Li et al., 2004). We expected L-Met to bind to both AtMAP1A and AtMAP2s, as the catalytic domains of these two enzymes displayed an extremely high level (>75%; see alignment in Giglione et al., 2000) of identity to HsMAP2 (Giglione et al., 2004). The 3D structure of Arabidopsis MAP2s was modeled based on the structure of HsMAP2 complexed with L-Met. The 3D structure of the active site of AtMAP1A was modeled from the 3D structure of *Escherichia coli* MAP (EcMAP) complexed with L-Met. The models generated showed overlapping 3D folds of the active site of both MAP types when shown in the same orientation (Fig. 3A). They also revealed that all the residues involved in L-Met recognition were conserved in both plant MAP types, with the exception of Cys-59, which was replaced by an Ala in AtMAP1A (Fig. 3A). This substitution does not interfere with substrate or L-Met analog recognition (Li et al., 2004).

L-Met impairs the growth of a *map1A* yeast line by inhibiting MAP2 in the millimolar range of concentration (Dummitt et al., 2003). Wild-type and *map1A-1* Arabidopsis seedlings were grown in the presence of equivalent amounts of L-Met. At a concentration of 2 mM L-Met, *map1A-1* KO plants displayed strongly impaired development (Fig. 3B). Increasing the concentration of L-Met blocked development completely. These data suggested that AtMAP2s could be inhibited by L-Met in vivo. Nevertheless, L-Met caused wild-type plants to grow more slowly (Fig. 3B). We concluded that the inhibition of wild-type seedling growth by L-Met may have resulted from either (1) nonselective inhibition of both cytoplasmic MAP types, suggesting that cytosolic NME is essential; or (2) the metabolism of L-Met to generate compounds that play a major role in the plant (Ravanel et al., 1998), for which changes in concentration could retard plant development. Hence, to delineate the role of cytosolic NME, an inhibitor with no effect on wild type was required.

Modulating MAP2 Activity with Fumagillin Affects Plant Development in the *map1A-1* Context

Fumagillin is a natural compound produced by the fungus *Aspergillus fumigatus* (McCowen et al., 1951). Fumagillin and its derivatives, such as TNP-470 (also known as AGM-1470; Ingber et al., 1990), fumagillone (compound 4 in Turk et al., 1998), or ovalicin (Corey et al., 1994), specifically and covalently bind and inactivate MAP2s, with low nanomolar binding con-

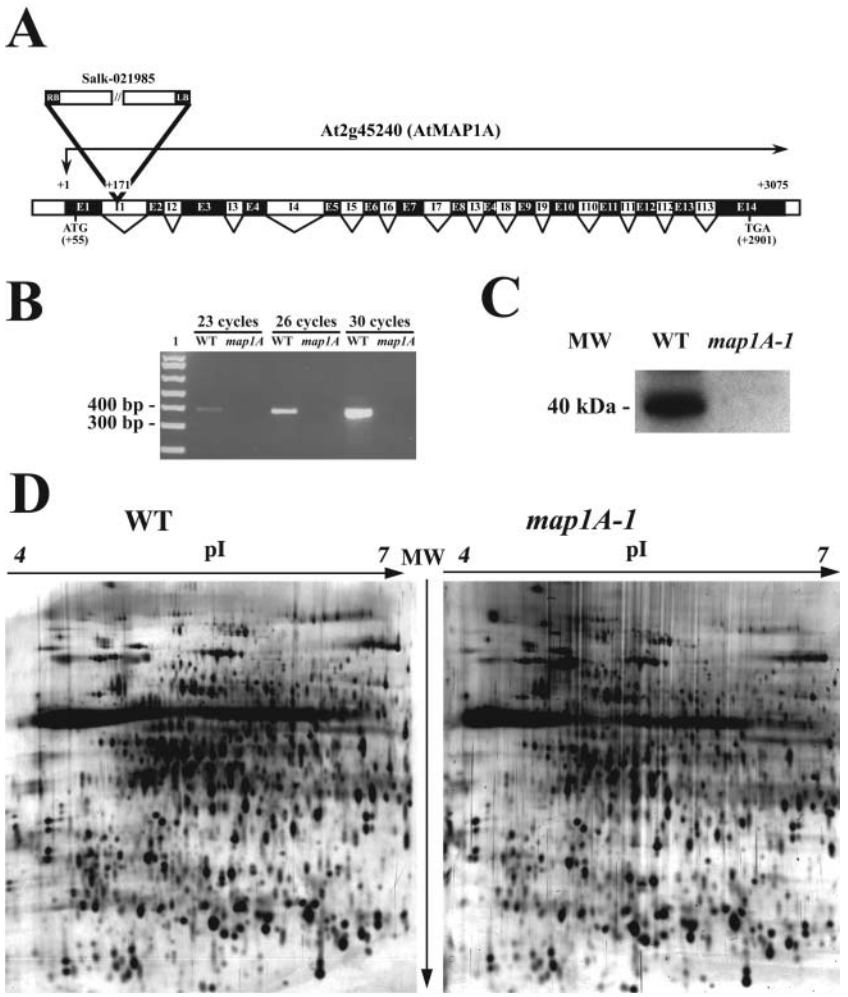

Figure 2. Characterization of a *map1A-1* plant line. A, Schematic representation of *MAP1A* gene disruption in Arabidopsis line SALK_021985 (*map1A-1*). The exon-intron structure of the gene is shown. Translation initiation and termination codons are indicated. The T-DNA insertion is shown with the border sequences of the insert (LB and RB) labeled to indicate the orientation of the insertion. The location of T-DNA end insertion was checked by DNA sequencing, PCR amplification, and restriction fragment length analysis. LB, Left border; RB, right border. B, RT-PCR analysis showing the absence of the *MAP1A* transcript in line *map1A-1*. *MAP1A* expression analysis in *map1A-1* and wild-type lines was performed by RT-PCR analysis using cDNA of either line as template. cDNA synthesis is described in "Materials and Methods." The amount of cDNA to be used in each experiment (about 2 ng) was estimated by real-time PCR analysis to yield the same amplification level for *EF1A*. The *MAP1A* cDNA-specific primers used in this experiment were 5′-CAGATGCATCGAGCATTGCTACTCTTTCCTGTC and 5′-ATTCGGTTCAACTTTGGGAGTCCCATC and were expected to yield a 382-bp amplification band. The DNA ladder (lane 1) corresponded to the 1-kb plus ladder (Bio-Rad). For each cDNA (wild type or *map1A*), the amplification resulting from three distinct cycle numbers (23, 26, and 30) is shown. C, Western-blot analysis of 10-DAI-old seedlings. WT, Wild type. We analyzed 80-μg aliquots of total protein by 10% denaturing PAGE, followed by electroblotting and probing of the resulting membrane with anti-MAP1A antibody. D, 2-DE patterns of wild type (left) and line *map1A-1* (right). MW, Molecular weight (M_r). The lowest molecular mass visible in the second dimension was 21 kD. The image shown is the most representative of the various experiments performed knowing that quantitative differences for the high-M_r spots were observed in various analysis of the same protein extract.

stants, but have no physiological effect on MAP1s (Griffith et al., 1997, 1998; Sin et al., 1997; Liu et al., 1998; Turk et al., 1998; Brdlik and Crews, 2004). The chemical structure of these four related compounds is shown in Figure 4A. As fumagillin has been shown to strongly inhibit all MAP2s tested, both in vitro and in vivo, and as we identified no particular phenotype with either *Ψmap* RNAi transgenic plant lines or the KO mutant line *map1A-1*, we thought to use this drug to investigate further the role of cytoplasmic NME in Arabidopsis in vivo. The 3D structure of Arabidopsis MAP2s with fumagillin was modeled from that of HsMAP2 complexed with fumagillin (Liu et al., 1998). This 3D model (Fig. 4B) revealed that all the residues involved in fumagillin recognition, including the crucial His residue (His-231; see Fig. 4B) responsible for covalent attachment of the drug, were conserved in both plant MAP2s. The only nonidentical residue was the Phe-366 of HsMAP2, which was replaced by a Cys in AtMAP2A. However, it was recently demonstrated

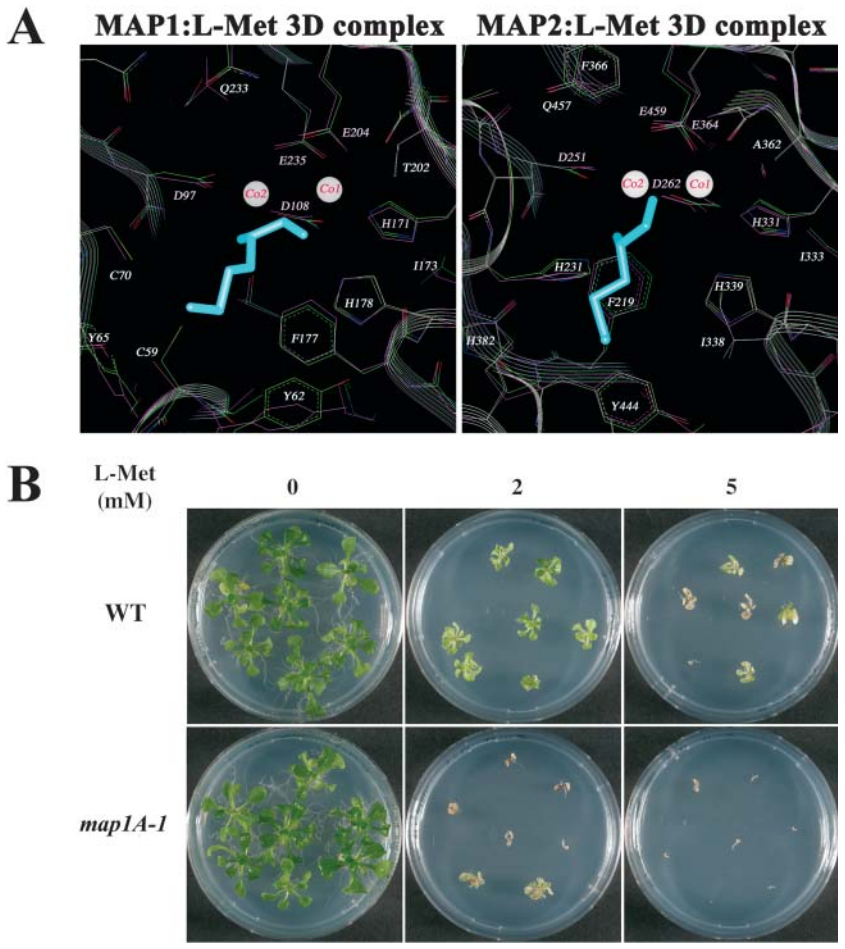

Figure 3. Challenging cytosolic NME with L-Met. A, In silico model of the active binding sites of AtMAP2 and AtMAP1A bound to L-Met. The structure of L-Met is indicated by blue sticks. A closeup of the active site of cytosolic MAP1 (left) and MAP2 (right), in the vicinity of the metal cation, is shown in the same orientation. The numbering and nature of residues is indicated in white (substrate-binding pocket) and pink (metal ligands). The two cobalt cations (Co1 and Co2) are shown as gray spheres. Hydrogen atoms are not shown. Left, The model structure of AtMAP1A is shown in purple and the crystal structure of EcMAP in green. Right, Model structure of AtMAP2B is shown in purple and the crystal structure of HsMAP2 in green. B, Effect of L-Met on plant growth. Wild-type or *map1A-1* plant lines were grown in the presence of the indicated (top) concentration of L-Met for 2 weeks.

that the Phe-366Cys substitution has no effect on the binding of fumagillin to HsMAP2 (Brdlik and Crews, 2004). The greater specificity of fumagillin for both AtMAP2s than for AtMAP1A was fully expected as AtMAP1A (1) has the Thr residue (Thr-202) involved in fumagillin selectivity between MAP1 (Ala-362) and MAP2 (Fig. 3A; Brdlik and Crews, 2004); and (2) possesses a Cys residue (Cys-70) rather than the crucial His-231 of MAP2s (Figs. 3A and 4B). These residues are conserved in all Arabidopsis MAP1s, including the three organellar isoforms (Giglione et al., 2000). Fumagillin, a commercially available compound, therefore appeared to be a useful chemical tool for the specific inhibition of both cytosolic MAP2 activities in plants.

Arabidopsis seeds were therefore sown in the presence of various concentrations, up to 15 μM, of fumagillin. No effects on wild-type plants (Fig. 4C) were observed, indicating that this drug did not impair plant development at the concentrations used and did not inhibit any essential target protein. When line *map1A-1*, which produced only MAP2A and MAP2B, the putative fumagillin-sensitive isoforms, was grown under similar conditions, it was found to be highly sensitive to the drug (Fig. 4C). Similar data were obtained when TNP-470, fumagillone, or ovalicin were used (Fig. 4, A and D). In contrast, actinonin, a specific inhibitor of organellar NME that blocks peptide deformylase activity (Giglione and Meinnel, 2001; Serero et al., 2001; Giglione et al., 2003), had no effect within the same range of concentration (data not shown). These results are consistent with fumagillin being highly specific for the two MAP2s and demonstrate that the effect observed is dependent on MAP2 inhibition only. At extremely low concentrations (0.01 μM) of fumagillin, line *map1A-1* displayed a dwarf phenotype (Fig. 4E) with very few secondary roots. These plants continued to grow slowly in the presence of the drug but developed a bushy leaf appearance (data not shown). Increasing the concentration of fumagillin increased the severity of the mutant phenotype, together with the effects on the root system. Finally, a strong block in development after germination was observed at fumagillin concentrations exceeding 1 μM (Fig. 4, C and F). These plants failed to turn green at or develop beyond the two-cotyledon stage. We compared wild-type and line *map1A-1* seeds sown in the presence of 1 μM fumagillin with a wild-type or a *map1A-1* mature embryo sown in the absence of the drug in which the primary seedling structure was morphologically recognizable and identified no structural differences. All

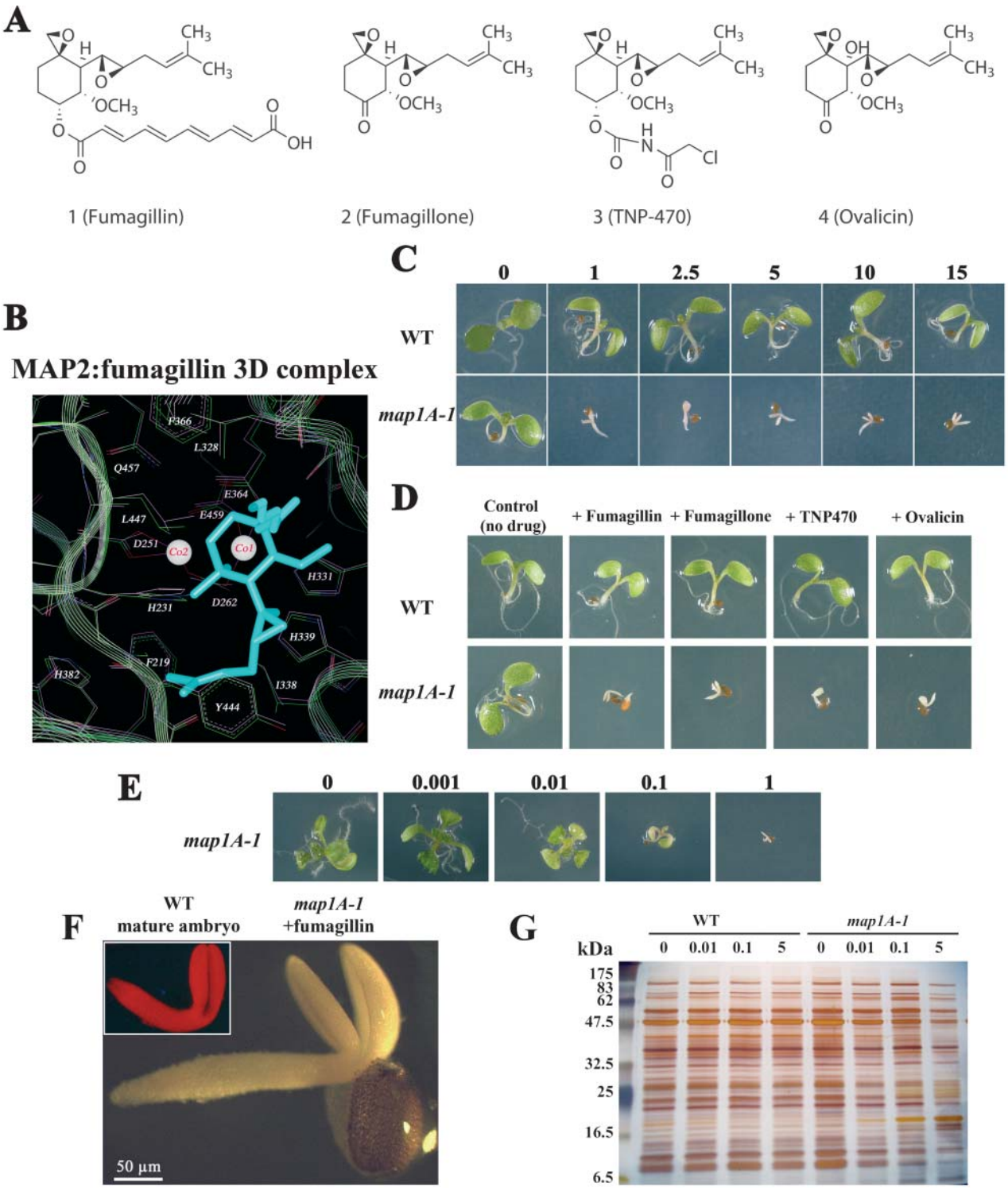

Figure 4. Fumagillin specifically targets and inhibits MAP2. A, Chemical structures of fumagillin and various structural analogs showing potent inhibition of MAP2. B, In silico model of the active binding site of AtMAP2B bound to fumagillin. See details in Figure 3A. The structure of fumagillin is indicated with blue sticks. Links between the metal cations and protein side chains are shown as red lines. The orientation of the fumagillin molecule is upside-down compared to A. C, 2-DAI-old wild-type or *map1A-1* line plants grown in the presence of the indicated (top) concentration of fumagillin (micromolar). D, 10-DAI-old *map1A-1* line plant grown in the presence of 5 μM of the indicated drug (structure shown in A). E, 10-DAI-old *map1A-1* line plant grown in the presence of the indicated (top) concentration of fumagillin (micromolar). F, Comparison of the size and morphology of a wild-type mature embryo stained with di-acetate fluorescein (top left inset) with a *map1A-1* line seedling germinating in the presence of 1 μM fumagillin. The scale for both is shown below the figure. G, 1D PAGE (12%) analysis of protein extracts originating from Arabidopsis plant lines (wild type or *map1A-1*) grown in the presence of the indicated concentration of fumagillin (micromolar). The gel was silver stained (Amersham). Molecular mass ranges corresponding to the first lane are indicated on the left border of the gel (Biolabs).

major structures were detected, including root, hypocotyls, and cotyledons, in both plants (Fig. 4F), indicating that MAP2 activity alone was sufficient for embryo formation but that development could not progress much beyond the mature embryonic stage if this activity was also inhibited. This suggested that fumagillin impaired cell expansion and the few early cell divisions in line *map1A-1*.

Next, experiments were performed with protein samples extracted from the *map1A-1* or wild-type lines grown in the absence or presence of 1 μM fumagillin (i.e. a concentration allowing complete inhibition of both MAP2 activities in fungi). When one-dimensional (1D) or 2-DE experiments were performed with a wild-type plant grown in the presence of 1 μM fumagillin, no discrepancy was observed compared to the control, and the patterns were similar to those shown in Figure 2D. This indicated that the absence of MAP2 activity was likely to be compensated by that of MAP1A. In contrast, the protein pattern of line *map1A-1* grown in the presence of more than 0.01 μM fumagillin was significantly modified compared to the control, as expected for the inhibition of an essential process that involves a majority of the proteins of the cytoplasm (Fig. 4G).

Thus, fumagillin specifically targets and inhibits both MAP2A and MAP2B, but not MAP1A, in plants. Moreover, our data indicate that (1) cytoplasmic NME (i.e. MAP1A + MAP2A + MAP2B activity) is an essential process in plants; (2) the function of both cytosolic MAP2 can be compensated by that of MAP1A; and (3) in the absence of MAP1A, the intrinsic level of MAP2 activity is crucial for correct development. As plant lines grew normally and showed identical protein patterns in the absence of either cytosolic MAP-type activity (i.e. MAP1A or MAP2A/B), we concluded that the two MAPs were interchangeable in plants.

Complete Inhibition of MAP2 Causes a Range of Developmental Perturbations in Plant Lines Producing Various Amounts of MAP1A

Having evaluated the impact of MAP2 activity on Arabidopsis cytoplasmic NME in genetic backgrounds devoid of MAP1A proteins, we then investigated the contribution of MAP1A proteins to this process. We sowed all the *Ψmap1A and Ψmap2* lines separately in a growth medium containing the concentration of fumagillin previously shown to yield the maximal effect in line *map1A*-1 (5.4 μM). We used concentrations of fumagillin up to that used in the experiments with *map1A-1* lines that completely blocked plant development, suggesting that the activity of the two MAP2 enzymes was completely inhibited. Seeds from wild-type plants, *ctl*, and *Ψmap2* T_1 lines germinated and developed normally on fumagillin (Fig. 5A), with normal dark-dependent skotomorphogenesis (data not shown). In contrast, developmentally abnormal plants were observed in the progeny of all the *Ψmap1A* lines grown in the presence of the drug. The most extreme phenotype, which was observed at various frequencies in the progeny from all *Ψmap1A* T_1 lines, was a complete block of plant development after emergence from the seed (Fig. 5A). The plants failed to turn green or to develop beyond the stage indicated and closely resembled *map1A-1* plants grown in the presence of high concentrations of the drug (see Fig. 4, C and E). Nevertheless, most of the progeny from the most affected *Ψmap1A* T_1 lines grown in the presence of fumagillin displayed a lesser effect on the roots than was observed in KO *map1A-1* plants (Fig. 4C).

The progeny from some of the *Ψmap1A* T_1 lines showed a gradient of less severe phenotypes on fumagillin medium than that typified by the complete developmental arrest occurring before leaf emergence. Such less extreme phenotypes included discolored and malformed cotyledons and leaves (Fig. 5B; see also Fig. 6) and slow growth. Such plants never reached the flowering stage. Light is known to cause an inhibitory effect on hypocotyl elongation. Because light-grown *map1A-1* and *Ψmap1A* seedlings in the presence of fumagillin showed extremely reduced hypocotyl elongation, we examined whether the hypocotyl was able to elongate in the dark. Similarly to wild type, all *Ψmap1A* seedlings had strong elongation of the hypocotyl when grown in the dark in the absence of the drug (Fig. 5C). However, the most severely affected *Ψmap1A-1* seedlings failed to exhibit hypocotyl elongation, even by 10 DAI in the dark (Fig. 5C), when grown in the presence of fumagillin. This indicated that *Ψmap1A* was severely defective in hypocotyl cell expansion/elongation and not responsive to dark treatment.

We assessed the correlation of *MAP1A* transcripts with the mutant phenotype. We used semiquantitative RT-PCR to determine *MAP1A* transcript levels in progeny plants of the same age from a single T_1 *Ψmap1A* line sown on fumagillin, which expressed the RNAi construct and displayed a severe or intermediate mutant phenotype or appeared normal. The values obtained were compared with those for wild-type and *ctl* T_1 progeny plants of equivalent age, producing RNAi transcripts, and sown on fumagillin. *MAP1A* transcript levels clearly decreased with increasing severity of the mutant phenotype (Fig. 5, B and D). These results are consistent with those reported for *map1A-1* KO plants (Fig. 4) in that these data demonstrate the need for a minimal level of cytoplasmic MAP activity for correct plant development. However, the greater sensitivity of *map1A-1* KO plant roots to fumagillin than of *Ψmap1A* lines suggests that a small amount of MAP1A can still ensure root development.

The Fumagillin-Induced NME Inactivation Phenotype Can Be Mimicked in an RNAi Plant Line Targeting the Complete Set of Cytoplasmic MAPs

We thought it should be possible to obtain viable transgenic plant lines displaying the above-described gradient of developmental arrest phenotypes by simultaneously using RNAi-mediated targeting of all cytoplasmic MAP transcripts with a single construct.

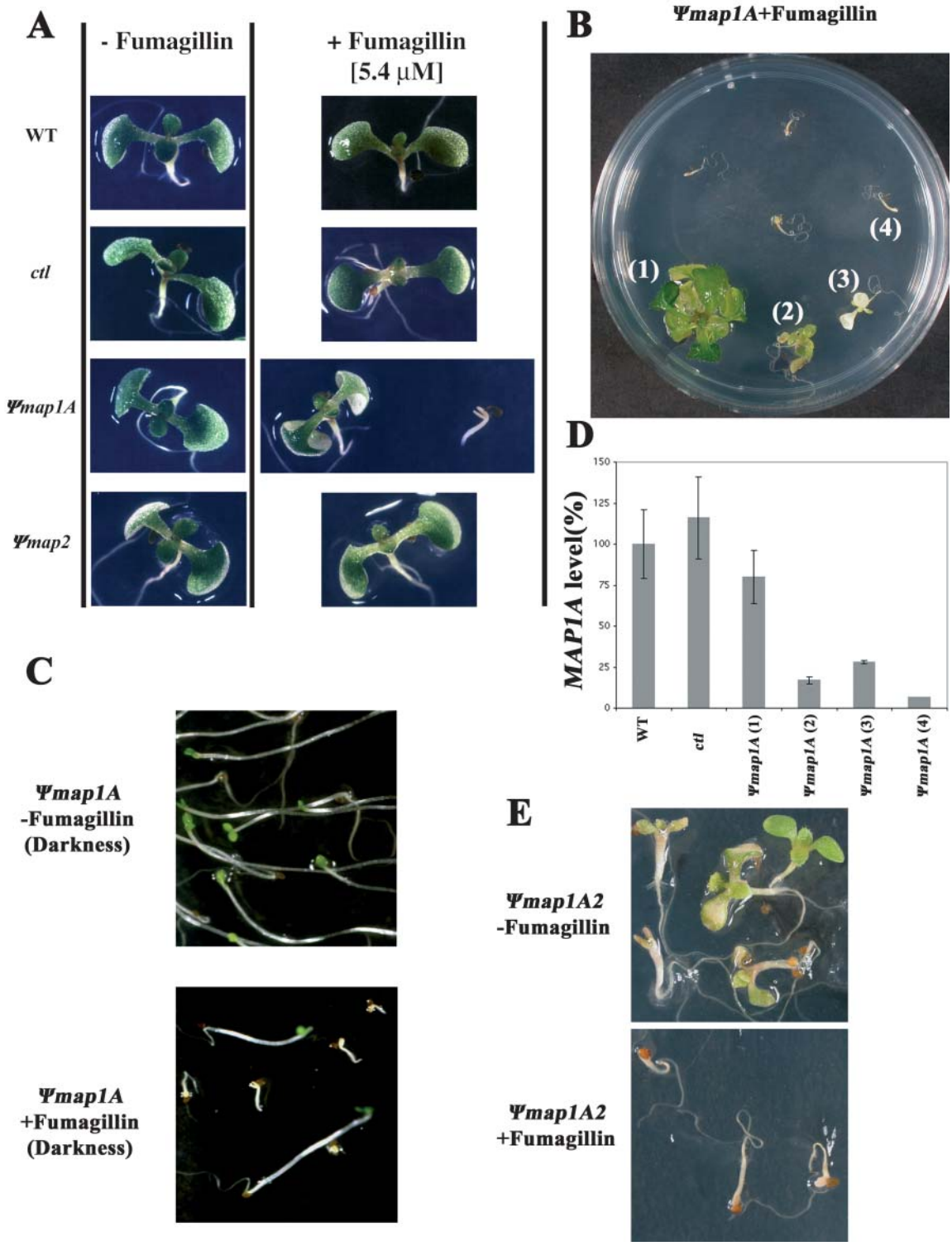

Figure 5. A gradient of developmental mutant phenotypes induced by fumagillin in *Ψmap1A* RNAi plant lines, according to *MAP1A* transcript levels. Various RNAi plant lines were grown in the presence or absence of the indicated concentration of fumagillin. WT, Wild type; *ctl*, corresponds to the control line (see text). A, Three-DAI-old T_1 progeny. The most divergent phenotypes attainable in the T_1 *Ψmap1A* progeny are shown. B, The T_2 progeny from a T_1 *Ψmap1A* line was sown on fumagillin. (X) indicates various plants for which *MAP1A*, *MAP2B*, and *MAP2A* RNA levels were analyzed. C, *Ψmap1A* T_1 progeny grown in the dark for 10 DAI in the absence (top) or in the presence (bottom) of 5.4 μM fumagillin. D, *MAP1A*/*EF1A* RNA levels of the plants selected in B, with wild-type values set to 100. E, Triple RNAi lines (*Ψmap1A2*) were grown for 10 DAI in the presence or absence of 5.4 μM fumagillin.

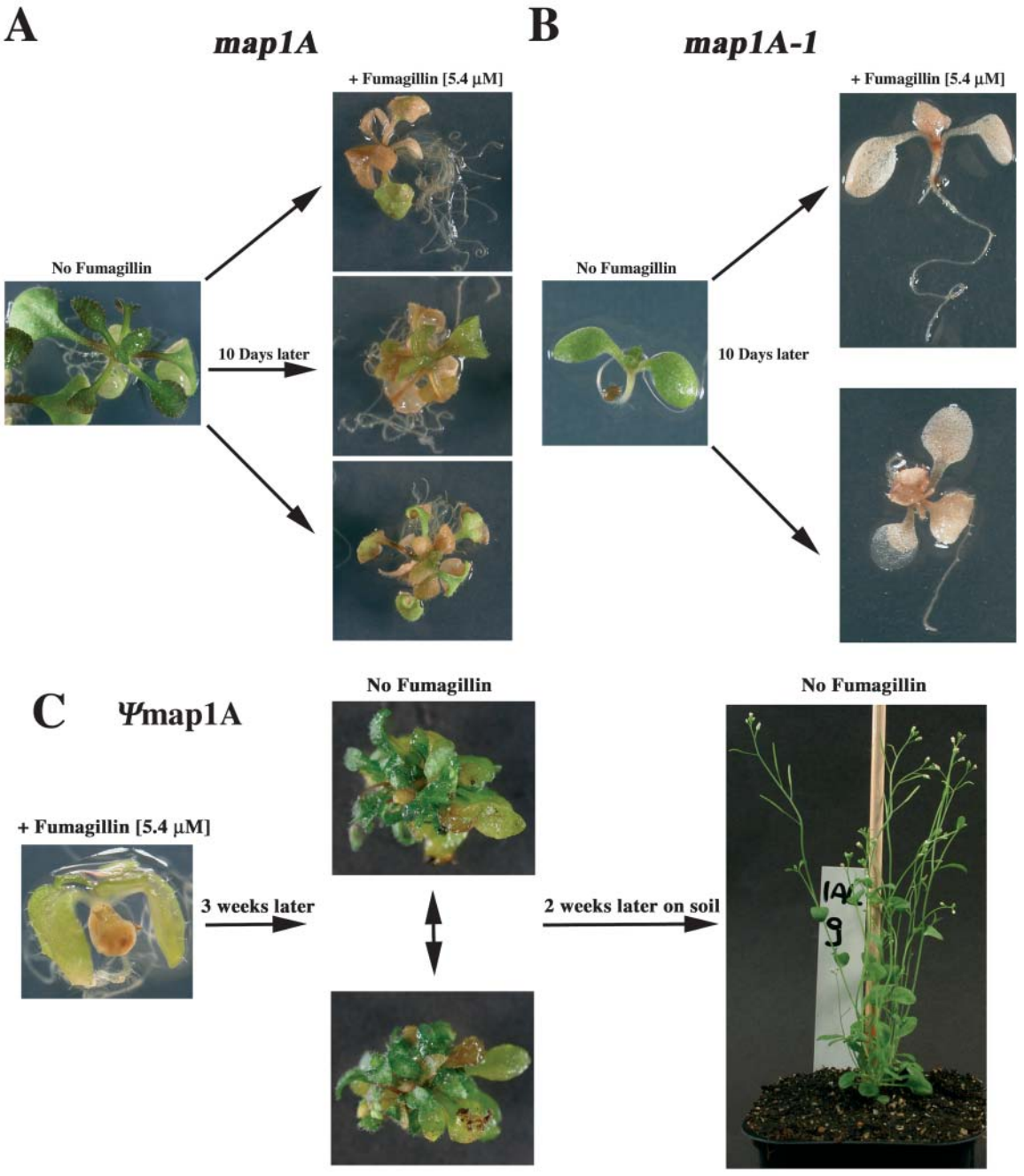

Figure 6. Reversible and irreversible effects of fumagillin on Arabidopsis *Ψmap1A* and *map1A-1* seedlings, respectively. Arabidopsis *Ψmap1A* or *map1A-1* seeds were sown in a growth medium without fumagillin, synchronized in the dark at 4°C for 2 DAI, and then incubated in a growth cabinet. Representative seedlings were photographed before and after sowing in the presence of the indicated concentration of fumagillin. A, *Ψmap1A* seedlings grown for 15 DAI before the addition of fumagillin. B, *map1A-1* seedlings grown for 3 DAI before the addition of fumagillin. C, Three-week-old *Ψmap1A* T_1 plants previously grown on 5.4 μM fumagillin and with a mild phenotype (left) were transferred to fumagillin-depleted growth medium for 3 more weeks (middle). The seedlings were then planted in soil and photographed 2 weeks later (right).

In the absence of fumagillin, the progeny of 11 out of 22 randomly selected Finale-resistant T_1 lines (*Ψmap1A2*) displayed the range of mutant phenotypes characteristic of *Ψmap1A* T_1 lines sown on fumagillin (Fig. 5E), with a milder effect on roots than observed with the *map1A-1* KO line (Fig. 4, C and E). However, fumagillin increased the number of mutants with the most severe phenotype. This was demonstrated when the progeny from four T_1 *Ψmap1A2* construct lines, together with wild-type plants and the progeny of

a strong mutant phenotype (observed with fumagillin) *Ψmap1A* T_1 line as controls, were grown in the presence or absence of fumagillin. These data confirmed our aforementioned conclusions on the essential role of NME in plant development. When transferred to soil, the least severely affected *Ψmap1A2* T_2 lines gave rise to plants with multiple emerging primary inflorescence of similar sizes (data not shown).

Irreversible and Reversible Effects of Postgermination NME Inactivation on Plant Development

We investigated whether the cytoplasmic NME machinery was crucial for plant development in *Ψmap1A* plants sown directly on fumagillin either because this machinery was inhibited from the beginning of plant growth or because it also plays a role in later developmental stages. Our demonstration that fumagillin specifically inhibited the two MAP2s and the construction of KD and KO *map1A-1* plant lines provided us with appropriate tools for specific cytoplasmic NME inactivation at any developmental stage. Two-week-old *Ψmap1A* lines previously grown in the absence of fumagillin were transferred to a medium containing 5.4 μM of this drug. Under these conditions, in plant lines with very low *MAP1A* transcript levels, the drug slowed down development and plants prematurely underwent senescence, leading to the formation of necrotic lesions on the leaves (Fig. 6A). No effect was observed in *Ψmap1A* lines containing larger amounts of this transcript. In *map1A-1* KO lines, we observed an almost immediate block of development, accompanied by rapid senescence of the apical region (Fig. 6B).

We then investigated the effects of transferring the progeny of *Ψmap1A* T_1 lines to fumagillin-free medium to determine whether the effects of this drug were reversible. Three-week-old *Ψmap1A* T_1 lines previously grown on fumagillin medium were transferred to fumagillin-depleted growth medium. Those with the most severe mutant phenotypes, similar to line 4 in Figure 5B, did not recover on fumagillin-free medium (data not shown). In contrast, mutants that had continued to develop, but slowly, similar to line 2 in Figure 5B, developed a bushy leaf appearance on transfer to fumagillin-free medium (Fig. 6C, middle), with shoots unable to grow upward away from the medium. These less severely affected mutants produced a large number of axillary buds rather than a single apical bud. Consistent with these findings, multiple inflorescences emerged following transfer to soil (Fig. 6C, right), rather than the more usual single main inflorescence, as seen in wild-type plants. Similar, but more marked phenotypes were observed with *map1A-1* lines: the higher the initial concentration of fumagillin, the longer the delay observed in the transition from the vegetative to the flowering stage. These results indicate that NME is crucial for development after the initial germination stages and that the plant can recover from an inhibited NME system, but with perturbed development.

DISCUSSION

The general mechanism of action of MAPs has been extensively studied in yeast and bacteria and the removal or retention of the initiator Met seems to be directed by the second residue (for review, see Giglione et al., 2004). MAPs cleave the N-terminal L-Met only if the second residue is small. Hence, by means of MAP substrate specificity, NME contributes to the diversity of the N-terminal amino acids occurring in mature proteins.

MAP2s Versus MAP1s: Overlapping or Redundant Functions in Higher Eukaryotic NME?

In the cytoplasm of eukaryotes, two different MAP types, MAP1 and MAP2, exist. The significance of the occurrence of two types of MAPs is unclear. In yeast, the only organism in which this issue has been addressed, MAP1 is the dominant isoform; inactivation of *MAP1* results in a slow-growth phenotype, whereas *MAP2* inactivation has no great effect. These data suggest that MAP2 is redundant, with MAP1 the chief enzyme in fungal NME (Dummitt et al., 2003). Recent data have suggested that the catalytic efficiencies of MAP1 and MAP2 might be slightly different in vivo for some substrates (Turk et al., 1999). For example, in yeast, MAP1 is the most efficient enzyme in NME, whereas MAP2 increases the efficiency of this process for some substrates only if overproduced (Chen et al., 2002). However, both MAPs were less efficient if the second residue was Val, and MAP2 was less efficient than MAP1 if the second residue was Cys, Gly, or Thr.

The importance of these MAPs in animal cell growth and tumor progression has been investigated, particularly since the identification of MAP2 as the molecular target for the antiangiogenic agent fumagillin and the discovery that this enzyme has POEP activity. Fumagillin and its derivatives specifically block the NME activity of MAP2, selectively inhibiting endothelial cell proliferation by arresting the cells in the G1 phase (Zhang et al., 2000). The mechanism underlying this selective inhibition remains unclear. Recent data suggest that MAP2 is tightly regulated throughout development and tumorigenesis. Regulation has been shown to occur at the transcriptional and post-transcriptional levels. MAP2 seems to accumulate in a cell- and tissue-specific manner. In insects, MAP2 transcripts are uniformly distributed during early embryonic development, but at later stages, they accumulate only in specific tissues (Cutforth and Gaul, 1999). MAP2 seems to be strongly and selectively expressed in germinal center B cells and some neoplastic cells, such as B-cell lymphoma cells, hepatoma cells, and mesothelioma cells (Wang et al., 2000; Catalano et al.,

2001; Kanno et al., 2002). These findings are consistent with the observation that MAP2 (p67) expression is inhibited in starved mammalian cell cultures and induced in proliferating cells (Gupta et al., 1997). Finally, MAP2 KD by RNAi caused germ cell proliferation defect in the worm *Caenorhabditis elegans* (Boxem et al., 2004).

The existing data for higher eukaryotes are slightly at odds with those for yeast. To reconcile these results, it has been suggested that free Met inhibits MAP2 activity (Dummitt et al., 2003). Met concentration in the yeast cytosol is close to the binding constant for MAP2 (0.1–1 mM), accounting for the lesser role of MAP2 in this lower eukaryote. In contrast, in animal endothelial cells, Met concentration is in the range of 5 to 30 μM. Met is found at quite similar low concentrations (approximately 15 μM) in plants (Shen et al., 2002) and this concentration is tightly controlled (Ravanel et al., 1998). The low concentration of free Met in the cytosol may make it possible for MAP2 to play a greater role in higher eukaryotes, including plants. However, a low cellular Met concentration alone cannot account for the tissue selectivity of fumagillin in mammalian cells. We clearly know too little about MAP1 expression in higher eukaryotes to draw any clear conclusions as yet. A decrease in total MAP activity or an increase in the demand for NME in specific tissues, such as angiogenic cells, might account for such observations. The blocking of MAP2 activity would probably lead to the retention of Met in a limited number of proteins. Proteins starting Met-Val would probably be affected in this way as they are already known to be in the least efficiently processed category for both MAPs. In any case, the down-regulation or inhibition of MAP2 activity would probably result in the production of some proteins with unprocessed N termini.

What the Plant Genetic System Contributes to Our Understanding of the Function of Cytoplasmic NME

To understand the roles of the two types of MAP enzyme in cytoplasmic NME, we need to modulate the activity of each type of MAP separately in a whole-cell system or in a whole, developing organism. This study of the cytoplasmic NME and the roles of MAP1 and MAP2 in a higher eukaryote is uncommon in that it is essentially based on the availability of: (1) a higher eukaryotic system devoid of MAP2-borne POEP activity; (2) a KO for cytoplasmic MAP1 (line *map1A-1*); and (3) a dual-compatibility epigenetic control system combining RNAi-triggered KD lines and drug susceptibility, making it possible to induce a loss-of-function or gain-of-function of all cytoplasmic MAPs at various developmental stages. We were therefore able to modulate NME production and activity at any time point. Various MAP KD mutants (*Ψmap1A*, *Ψmap2*, and *Ψmap1A2*) were isolated. Lines *Ψmap1A*, *Ψmap2*, and *map1A-1* displayed a wild-type phenotype, indicating that the two types of MAPs are fully interchangeable in plants. Our data show that plant MAP2s do not have POEP activity, as predicted from examination of their N-terminal domains. If these enzymes had POEP activity, line *Ψmap2* would display an apoptotic phenotype. Our data, showing that all *map1A-1* mutants were viable, and the observation of aberrant developmental phenotypes in the presence of L-Met or fumagillin suggest that MAP2 plays an expanded role in higher eukaryotes, as previously suggested. Our data also showed that cytoplasmic NME (i.e. MAP1A + MAP2A + MAP2B activity) as a whole is essential for plant development and that each individual component is dispensable, provided that other components are present. Finally, our data suggest that a true triple MAP KO mutant would be embryo lethal. These findings were confirmed by the occurrence of extremely severe mutant phenotypes in the triple RNAi lines. Moreover, in the absence of MAP1A, MAP2 levels become especially important for developmental progress, and root development in particular.

Recently, Kim et al. (2004) has proposed that human MAP2 is not the target for the antiangiogenic effect of fumagillin, suggesting that the drug could also target other important cellular molecules in animal epithelial cells. With the plant system, we found that fumagillin has no effect on wild-type and *Ψmap2* KD lines. This implies that the drug has no other antiproliferative target in Arabidopsis, confirming the strong specificity of fumagillin for MAP2, as reported in fungi and animals (Griffith et al., 1997, 1998; Sin et al., 1997). To get more insight into the specificity of fumagillin, we used several other drugs known to be highly specific for MAP2 and obtained similar results (Fig. 4D). Our data show that, in line *map1A-1*, MAP2 inhibition strongly impairs plant cell elongation/expansion (Fig. 5D) and suggest that it also blocks cell division. This latter conclusion is in line with earlier reports describing the inhibitory effect of the fumagillin analog TNP-470 on animal cell cycle (Abe et al., 1994; Yeh et al., 2000; Zhang et al., 2000; Lien et al., 2004).

A gradient of developmentally abnormal plants was observed in the progeny of *Ψmap1A* lines grown in the presence of saturating concentrations of fumagillin, with a clear relationship between MAP1A content and phenotype severity. These mutants had a phenotype similar to that observed with *map1A-1* plants grown in the presence of various concentrations of fumagillin. However, the roots of these plants were less severely affected than those of *map1A-1* KO plants grown in similar conditions. The higher sensitivity of *map1A-1* KO plant roots to fumagillin than the *Ψmap1A* line in the presence of the drug suggests that MAP2 level or activity is limiting in this organ as a whole or in specific cell types. The much later flowering of the *map1A-1* KO line replanted in the absence of fumagillin, correlated with the initial concentration of fumagillin, is also consistent with these conclusions. Our results suggest that MAP1A plays a major role in root development and in the transition between the vegetative and reproductive stages. This effect is not due to

reduced MAP2 transcript levels in the roots. MAP2 transcript levels were found to be similar in different organs and these transcripts were the most abundant of the three *MAP* transcripts. The strong induction and accumulation of all three *MAP* transcripts, particularly those corresponding to *MAP1A*, at the beginning of plant development (Fig. 1A), together with the fumagillin-induced stimulation of senescence in *map1A-1* KO adult plants and the most severely affected *Ψmap1A* lines, suggest that adequate cytoplasmic NME in the leaves is essential for plant growth. Taking into account our results and those of cytoplasmic MAPs of other eukaryotes, we could speculate on various nonexclusive hypotheses. First, in specific tissues, MAP2 is somehow more strongly inhibited, for instance, by a local higher concentration of free Met, in keeping with our data showing Met-induced inhibition of NME (Fig. 3). Second, there are some specific or fastidious substrates whose accumulation is strictly required for defined plant development pathways, and for which NME can still be ensured by a low concentration of MAP1A but not of MAP2. This is in line with the data indicating that MAP1 and MAP2 exhibit different cleavage efficiencies against the same substrates in yeast (Dummitt et al., 2003). As a result, MAP2s will efficiently ensure the cleavage of these substrates if present at their physiological limiting concentration or if overproduced.

Our studies generate a model of the functions of the three components of cytoplasmic NME from a higher eukaryote. The demand for cytoplasmic NME increases during development, as revealed by the transcriptional induction of all three MAPs, especially MAP1A (Fig. 1A). Transcript levels are strictly controlled and kept constant by the induction of a given MAP in most organs, including those in which *MAP1A* transcription has been reduced or stopped, as in flowers and siliques. In siliques, to compensate for the disappearance of *MAP1A* mRNA, there is a strong induction of the otherwise minor MAP gene, *MAP2A*, thereby restoring optimal MAP levels. Thus, the plant tries to compensate for artificially reduced MAP levels by increasing the levels of other MAPs.

MATERIALS AND METHODS

Plants and Growth Conditions

Arabidopsis (*Arabidopsis thaliana*) ecotype Columbia seeds were surface sterilized and sown on 0.5× Murashige and Skoog (Sigma, St.-Quentin Fallavier, France) medium supplemented with 0.8% agarose (Becton Dickinson, Le Pont de Claix, France) and 1% Suc (Sigma). When a MAP2 inhibitor like fumagillin was used, all media, whatever the concentration of the drug, including the control without any MAP2 inhibitor, contained 0.05% methanol (final concentration). After sowing in petri dishes, seeds were imbibed for 2 d in the dark at 4°C for vernalization purposes. Petri dishes were next incubated in a growth chamber (22°C, 16 h of daylight, light intensity 100 μE m^{-2} s^{-1}) for up to 5 weeks. Plant growth kinetics were measured in DAI (i.e. the number of days of incubation in the growth chamber at 22°C). Arabidopsis lines were propagated under greenhouse conditions, as previously described (Giglione et al., 2000). Salk T-DNA insertion lines (Alonso et al., 2003), SALK_021985 (*map1A-1*) and two putative *map2B* lines, SALK_100162 and SALK_038477, were obtained from the Nottingham Arabidopsis Stock Centre (http://nasc.nott.ac.uk). We followed the usual recommendations for naming true KO plant lines (Meinke and Koornneef, 1997). RNAi plant lines with KD expression were named *Ψxyz-i* with *XYZ* corresponding to the name of the corresponding gene and each subline with a number (i or ii) following a dash. For instance, *Ψmap1A-i* refers to a given MAP1A KD line.

Materials and General Molecular Biology Methods

All chemicals were purchased from Sigma except TNP-470, ovalicin, and fumagillone, which were kindly provided by J.O. Liu (Baltimore). Fumagillin and its analogs were dissolved in 100% methanol as 10-mM solutions. Restriction enzymes and T4 DNA ligase were purchased from New England BioLabs (Ozyme, Saint-Quentin en Yvelines, France). The buffers used were those indicated by the manufacturer. Oligonucleotides were synthesized by MWG-BIOTECH (Courtaboeuf, France). Nucleotide sequences were determined by the big-dye terminator V3 method, with a 16-capillary ABI PRISM 3100 genetic analyzer (PE-Applied Biosystems, Courtaboeuf, France), using DNA templates purified with the QIAprep mini-prep or QIAquick gel extraction kits (Qiagen, Courtaboeuf, France). PCR was performed with Eurobiotaq II (Eurobio, Les Ulis, France), on an Omn-E thermal cycler (Hybaid, Coger, Paris), unless otherwise stated. All PCR-derived fragments for cloning were amplified with *Pfu* DNA polymerase (Stratagene, La Jolla, CA) and sequenced after cloning to check that they were identical to the original fragment. Southern blotting was performed as described elsewhere (Sambrook et al., 1989), using positive nylon membranes (Qbiogene, Illkirch, France). The Megaprime DNA labeling system (Amersham BioSciences, Orsay, France) was used to label probes with [α-^{32}P]-dCTP (Amersham), according to the manufacturer's instructions. Hybridization and posthybridization washes were systematically carried out under stringent conditions. Radioactive signals were detected and quantified on a Storm-840 phosphorimager (Amersham), using ImageQuant 5.2 software (Molecular Dynamics, Amersham).

Plant RNAi Constructs

A strategy similar to that previously described by Chuang and Meyerowitz (2000) was followed. First, three RNAi vectors, the first targeting *MAP1A*, the second targeting both *MAP2A* and *MAP2B*, and the third targeting the three cytosolic *MAP* genes, were constructed. Coding sequences were inserted as inverted repeats on either side of a β-glucuronidase (GUS) gene spacer, the whole sequence being transcribed under the control of a strong promoter (double-p35S) in the binary vector pMS101, facilitating selection on Finale (AgrEvo, Montvale, NJ), a phosphinothricin herbicide. A 280-bp sequence originating from the 5′ sequence of the cDNA encoding the MAP1A-specific zinc-binding domain was used (nucleotides 206–485; GenBank AF250960) to prevent the down-regulation of organellar *MAP1D* genes (see Table I). We used a 359-bp *MAP2B* cDNA sequence (nucleotides 598–956; GenBank AF300880) to target both *MAP2A* and *MAP2B* transcripts. This nucleotide sequence displays a high level of identity to the *MAP2A* sequence, with a significant number of identical stretches of 25 to 30 bp. We therefore fully expected both *MAP2*s to be targeted via dicer nuclease activity. Second, a construct including inverted *ctl* sequences (326 bp; nucleotides 298–623; EMBL V00618) was produced to serve as a control. RNAi constructs were generated by a two-step procedure in which the target gene-specific sequences were first amplified and cloned as inverted repeats on either side of an *Eco*RI/*Eco*RV fragment containing the GUS gene sequence (nucleotides 2,252–3,317; GenBank M14641) derived from plasmid pPR76. The inverted repeats separated by the GUS spacer sequence were then inserted into a plant transformation and expression vector, pMS101. Gene-specific fragments were amplified, using *MAP* cDNA fragments (Giglione et al., 2000) or plasmid pPR98 for the neomycin phosphotransferase gene (*nptII*) for control purposes, as templates. Complete details of the constructions are available (see supplemental material).

Constructs were used for the electrotransformation of Agrobacterium strain EHA105 (Hood et al., 1993), which was then used to transform Arabidopsis Columbia plants by the floral-dip method (Clough and Bent, 1998). Transgenic plants (T_1) were germinated and selected on sand continuously soaked with 10% Finale (AgrEvo) in the greenhouse. Resistant plants were transferred to soil at the two-leaf stage. The control line (*ctl*) corresponds to a line expressing the *nptII* inverted repeats instead of the given *MAP* constructs. Line *ctl* has no target for *nptII* inverted repeats.

Semiquantitative RT-PCR

Total RNA was prepared using the RNeasy kit (Qiagen) and treated with amplification grade DNase I (Invitrogen, Cergy-Pontoise, France) according to the manufacturer's instructions. We used approximately 350 ng of RNA for first-strand cDNA synthesis in the SuperScript system (Invitrogen), according to the manufacturer's instructions, using the provided oligo(dT) primer in the presence or absence (control) of the reverse transcriptase. Individual PCR reactions for each primer couple were carried out for three sets of different cycles. A logarithmic plot of signal strength for each cycle chosen was used to confirm that products were amplified in the linear range of the reaction.

We analyzed the *MAP1A* to *EF1A* transcript ratios in T_2 plants in which the *MAP1A* transcript was targeted. These plants displayed a range of mutant phenotypes with fumagillin. We sowed T_2 plants from one weak *Ψmap1A* line on fumagillin, along with T_2 plants from a *ctl* line and wild-type plants to act as controls. Plant tissues were harvested after the same amount of time of growth from each plant. For plants with a strong mutant phenotype, we collected all the material from a number of plants together. The presence of the inverted *nptII* gene sequences in *ctl* plant tissue was confirmed. The entire procedure for obtaining *MAP1A/EF1A* ratios was repeated at least three times, using different initial cDNA from various plants. For plants analyzed in the absence of fumagillin, total leaf and cotyledon material was collected from 10-DAI-old plants at the 2-leaf stage displaying equivalent development. We analyzed a single T_2 plant from each T_1 line and a wild-type plant in a single RT-PCR experiment, and the entire experiment was then repeated with a different set of plants. T_2 plants were selected at random from plants possessing both arms of the inverted *MAP* or *nptII* gene sequences. DNA was prepared as previously described (Edwards et al., 1991). Full details and oligonucleotide sequences are available (see supplemental data).

Real-Time Quantitative RT-PCR

Total RNA was extracted from Arabidopsis 10-DAI-old plants as previously described (Kay et al., 1987). Poly(A)$^+$ RNA was isolated on oligo(dT) 25 Dynabeads (Dynal, Compiègne, France). We then subjected 200 ng of mRNA to reverse transcription. The cDNA (about 2 ng) was then amplified by PCR, using the specific oligonucleotides. Real-time PCR was optimized with the LightCycler FastStart DNA Master SYBR Green kit (Roche, Meylan, France) for each primer pair (amplification efficiency was always >90%), using a standard cDNA. Each cDNA sample was quantified at least twice, with respect to a standard cDNA quantified in the same conditions. All experiments were performed with a LightCycler and the data were processed with LightCycler version 1.0 quantitative software (Roche). Full details and oligonucleotide sequences are available (see supplemental data).

3D Modeling of the Structures of Cytosolic MAPs from Arabidopsis

The amino acid sequences of AtMAP2A and AtMAP2B were aligned with that of HsMAP2 and the amino acid sequence of AtMAP1A was aligned with that of EcMAP, using InsightII software (Accelrys, San Diego). The 3D structures of HsMAP2 bound to fumagillin (PDB entry 1BOA; Liu et al., 1998) or L-Met (PDB entry 1KQ9) and EcMAP bound to L-Met (PDB entry 1C21; Lowther et al., 1999) were used to construct several 3D models of AtMAP2B and AtMAP1A with the homology modeler module. In each case, the lowest energy structure was further minimized with the CharmM forcefield and superimposed onto the structure of fumagillin or L-Met bound to HsMAP2 or EcMAP. We used the numbering systems of HsMAP2 and EcMAP to refer to the corresponding identical residues in AtMAP2B and AtMAP1A, respectively.

2-DE and Other Protein Analysis

The 8-DAI-old Arabidopsis plantlets were frozen in liquid nitrogen and disrupted in a MM 300 mixer mill (Qiagen). To extract total protein, the samples were resuspended in a prechilled 50 mM HEPES buffer, pH 7.2, containing 150 mM NaCl, 10% glycerol, 1.5 mM $MgCl_2$, 1% Triton X-100, 1 mM EGTA, 2 mM PMSF, and protease inhibitor cocktail (Roche) and incubated under agitation at 4°C for 1 h to allow solubilization. The supernatant was separated from the insoluble fraction by centrifugation at 13,300*g* at 4°C for 1 h.

For 2-DE, the supernatant was further purified with a Plus One 2D clean-up kit (Amersham). Protein concentrations were measured with the Bio-Rad (Marnes-La-Coquette, France) protein assay. Bovine serum albumin was used as the protein standard. For the first dimension, immobiline dry strips (18 cm; pH 4–7; Amersham) were rehydrated overnight in a solution (final volume 500 μL) containing 7 M urea, 2 M thiourea, 0.4% (v/v) immobiline pH gradient buffer 4 to 7 (Amersham), 0.2% Triton X-100, 2% (w/v) CHAPS, and 20 mM dithiothreitol plus the protein sample (400 μg) at 20°C. The hydrated strip was then electrofocalized for 4 h at 100 V followed by 4 h at 300 V, 12 h at 1,600 V, and finally by 7.5 h at 3,000 V at 20°C in a Protean IEF cell (Bio-Rad). For the second dimension, the strip was reequilibrated prior to separation by electrophoresis in SDS denaturing, 11% polyacrylamide gels (1 mm thick, 20 cm long), which was performed in a PROTEAN II *xi* cell (Bio-Rad). Protein silver staining was performed with a Plus One silver staining kit (Amersham). The gels were scanned with a GS800 imaging densitometer and analyzed with the PD-Quest 7.1 software (Bio-Rad). Each experiment was repeated at least four times.

Western blotting was performed as previously described (Giglione et al., 2003). To produce specific antibodies against MAP1A, a specific N-terminal fragment of MAP1A (codons 1–138) was overproduced in vector pET16B as a C-terminal His-tag fusion in strain Rosetta(DE3)pLysS (Novagen, VWR International, Fontenay-sous-Bois, France). The protein was purified on a Hi-Trap chelating HP (0.7 × 2.5 cm; Amersham) nickel affinity column. Rabbit antisera against AtMAP1A were raised by Eurogentec (Herstal, Belgium) and purified before use by differential ammonium sulfate precipitation and DEAE chromatography.

Upon request, all novel materials described in this publication will be made available in a timely manner for noncommercial research purposes, subject to the requisite permission from any third-party owners of all or parts of the material. Obtaining any permissions will be the responsibility of the requester.

ACKNOWLEDGMENTS

Dr. Jun O. Liu (Johns Hopkins University School of Medicine, Baltimore) is acknowledged for support, advice, and the gift of the various fumagillin analogs used in this study. We thank P. Ratet (Institut des Sciences du Végétal, France) for providing plasmids and advice.

Received November 19, 2004; returned for revision December 10, 2004; accepted December 10, 2004.

LITERATURE CITED

Abe J, Zhou W, Takuwa N, Taguchi J, Kurokawa K, Kumada M, Takuwa Y (1994) A fumagillin derivative angiogenesis inhibitor, AGM-1470, inhibits activation of cyclin-dependent kinases and phosphorylation of retinoblastoma gene product but not protein tyrosyl phosphorylation or protooncogene expression in vascular endothelial cells. Cancer Res **54:** 3407–3412

Alonso JM, Stepanova AN, Leisse TJ, Kim CJ, Chen H, Shinn P, Stevenson DK, Zimmerman J, Barajas P, Cheuk R, et al (2003) Genome-wide insertional mutagenesis of *Arabidopsis thaliana.* Science **301:** 653–657

Boisson B, Giglione C, Meinnel T (2003) Unexpected protein families including cell defense components feature in the N-myristoylome of a higher eukaryote. J Biol Chem **278:** 43418–43429

Boxem M, Tsai CW, Zhang Y, Saito RM, Liu JO (2004) The C. elegans methionine aminopeptidase 2 analog map-2 is required for germ cell proliferation. FEBS Lett **576:** 245–250

Bradshaw RA, Brickey WW, Walker KW (1998) N-terminal processing: the methionine aminopeptidase and N alpha-acetyl transferase families. Trends Biochem Sci **23:** 263–267

Brdlik CM, Crews CM (2004) A single amino acid residue defines the difference in ovalicin-sensitivity between type I and II methionine aminopeptidases. J Biol Chem **279:** 9475–9480

Catalano A, Romano M, Robuffo I, Strizzi L, Procopio A (2001) Methionine aminopeptidase-2 regulates human mesothelioma cell survival: role of bcl-2 expression and telomerase activity. Am J Pathol **159:** 721–731

Chang YH, Teichert U, Smith JA (1992) Molecular cloning, sequencing, deletion, and overexpression of a methionine aminopeptidase gene from *Saccharomyces cerevisiae.* J Biol Chem **267:** 8007–8011

Chen S, Vetro JA, Chang YH (2002) The specificity *in vivo* of two distinct

methionine aminopeptidases in *Saccharomyces cerevisiae*. Arch Biochem Biophys **398:** 87–93

Chuang CF, Meyerowitz EM (2000) Specific and heritable genetic interference by double-stranded RNA in *Arabidopsis thaliana*. Proc Natl Acad Sci USA **97:** 4985–4990

Clough SJ, Bent AF (1998) Floral dip: a simplified method for Agrobacterium-mediated transformation of *Arabidopsis thaliana*. Plant J **16:** 735–743

Corey EJ, Guzman-Perez A, Noe MC (1994) Short enantioselective synthesis of (-)-ovalicin, a potent inhibitor of angiogenesis, using substrate-enhanced catalytic asymmetric dihydroxylation. J Am Chem Soc **116:** 12109–12110

Cutforth T, Gaul U (1999) A methionine aminopeptidase and putative regulator of translation initiation is required for cell growth and patterning in Drosophila. Mech Dev **82:** 23–28

Datta B (2000) MAPs and POEP of the roads from prokaryotic to eukaryotic kingdoms. Biochimie **82:** 95–107

Dummitt B, Micka WS, Chang YH (2003) N-terminal methionine removal and methionine metabolism in *Saccharomyces cerevisiae*. J Cell Biochem **89:** 964–974

Edwards K, Johnstone C, Thompson C (1991) A simple and rapid method for the preparation of plant genomic DNA for PCR analysis. Nucleic Acids Res **19:** 1349

Giglione C, Boularot A, Meinnel T (2004) Protein N-terminal methionine excision. Cell Mol Life Sci **61:** 1455–1474

Giglione C, Meinnel T (2001) Organellar peptide deformylases: universality of the N-terminal methionine cleavage mechanism. Trends Plant Sci **6:** 566–572

Giglione C, Serero A, Pierre M, Boisson B, Meinnel T (2000) Identification of eukaryotic peptide deformylases reveals universality of N-terminal protein processing mechanisms. EMBO J **19:** 5916–5929

Giglione C, Vallon O, Meinnel T (2003) Control of protein life-span by N-terminal methionine excision. EMBO J **22:** 13–23

Griffith EC, Su Z, Niwayama S, Ramsay CA, Chang YH, Liu JO (1998) Molecular recognition of angiogenesis inhibitors fumagillin and ovalicin by methionine aminopeptidase 2. Proc Natl Acad Sci USA **95:** 15183–15188

Griffith EC, Su Z, Turk BE, Chen S, Chang Y-H, Wu Z, Biemann K, Liu J (1997) Methionine aminopeptidase (type 2) is the common target for angiogenesis AGM-1470 and ovalicin. Chem Biol **4:** 461–471

Gupta S, Bose A, Chatterjee N, Saha D, Wu S, Gupta NK (1997) p67 transcription regulates translation in serum-starved and mitogen-activated KRC-7 cells. J Biol Chem **272:** 12699–12704

Hood EE, Gelvin SB, Melchers LS, Hoekema A (1993) New Agrobacterium helper plasmids for gene transfer to plants. Transgenic Res **2:** 208–218

Ingber D, Fujita T, Kishimoto S, Sudo K, Kanamaru T, Brem H, Folkman J (1990) Synthetic analogues of fumagillin that inhibit angiogenesis and suppress tumour growth. Nature **348:** 555–557

Kanno T, Endo H, Takeuchi K, Morishita Y, Fukayama M, Mori S (2002) High expression of methionine aminopeptidase type 2 in germinal center B cells and their neoplastic counterparts. Lab Invest **82:** 893–901

Kay R, Chan A, Daly M, McPherson J (1987) Duplication of CaMV 35S promoter sequences creates a strong enhancer for plant genes. Science **236:** 1299–1302

Kendall RL, Bradshaw RA (1992) Isolation and characterization of the methionine aminopeptidase from porcine liver responsible for the co-translational processing of proteins. J Biol Chem **267:** 20667–20673

Killough JH, Magill GB, Smith RC (1952) The treatment of amebiasis with fumagillin. Science **115:** 71–72

Kim S, LaMontagne K, Sabio M, Sharma S, Versace RW, Yusuff N, Phillips PE (2004) Depletion of methionine aminopeptidase 2 does not alter cell response to fumagillin or bengamides. Cancer Res **64:** 2984–2987

Li JY, Cui YM, Chen LL, Gu M, Li J, Nan FJ, Ye QZ (2004) Mutations at the S1 site of methionine aminopeptidases from *Escherichia coli* and *Homo sapiens* reveal the residues critical for substrate specificity. J Biol Chem **279:** 21128–21134

Li X, Chang YH (1995) Amino-terminal protein processing in *Saccharomyces cerevisiae* is an essential function that requires two distinct methionine aminopeptidases. Proc Natl Acad Sci USA **92:** 12357–12361

Lien WH, Chen CK, Lai LY, Chen YH, Wu MP, Wu LW (2004) Participation of cyclin D1 deregulation in TNP-470-mediated cytostatic effect: involvement of senescence. Biochem Pharmacol **68:** 729–738

Liu S, Widom J, Kemp CW, Clardy J (1998) Structure of human methionine aminopeptidase-2 complexed with fumagillin. Science **282:** 1324–1327

Lowther WT, Matthews BW (2002) Metalloaminopeptidases: common functional themes in disparate structural surroundings. Chem Rev **102:** 4581–4608

Lowther WT, Zhang Y, Sampson PB, Honek JF, Matthews BW (1999) Insights into the mechanism of *Escherichia coli* methionine aminopeptidase from the structural analysis of reaction products and phosphorus-based transition-state analogues. Biochemistry **38:** 14810–14819

McCowen MC, Callender ME, Lawlis J Jr (1951) Fumagillin (H-3), a new antibiotic with amebicidal properties. Science **113:** 202–203

Meinke D, Koornneef M (1997) Community standards for *Arabidopsis* genetics. Plant J **12:** 247–253

Meinnel T, Mechulam Y, Blanquet S (1993) Methionine as translation start signal: a review of the enzymes of the pathway in *Escherichia coli*. Biochimie **75:** 1061–1075

Ravanel S, Gakiere B, Job D, Douce R (1998) The specific features of methionine biosynthesis and metabolism in plants. Proc Natl Acad Sci USA **95:** 7805–7812

Ray MK, Datta B, Chakraborty A, Chattopadhyay A, Meza-Keuthen S, Gupta NK (1992) The eukaryotic initiation factor 2-associated 67-kDa polypeptide (p67) plays a critical role in regulation of protein synthesis initiation in animal cells. Proc Natl Acad Sci USA **89:** 539–543

Sambrook J, Fritsch EF, Maniatis T (1989) Molecular Cloning: A Laboratory Manual, Ed 2. Cold Spring Harbor Laboratory Press, Cold Spring Harbor, NY

Serero A, Giglione C, Meinnel T (2001) Distinctive features of the two classes of eukaryotic peptide deformylases. J Mol Biol **314:** 695–708

Serero A, Giglione C, Sardini A, Martinez Sanz J, Meinnel T (2003) An unusual peptide deformylase features in the human mitochondrial N-terminal methionine excision pathway. J Biol Chem **278:** 52953–52963

Shen B, Li C, Tarczynski MC (2002) High free-methionine and decreased lignin content result from a mutation in the Arabidopsis S-adenosyl-L-methionine synthetase 3 gene. Plant J **29:** 371–380

Sin N, Meng L, Wang MQ, Wen JJ, Bornmann WG, Crews CM (1997) The anti-angiogenic agent fumagillin covalently binds and inhibits the methionine aminopeptidase, MetAP-2. Proc Natl Acad Sci USA **94:** 6099–6103

Towbin H, Bair KW, DeCaprio JA, Eck M, Kim S, Kinder FR, Morollo A, Mueller DR, Schindler P, Song HK, et al (2003) Proteomics based target identification: bengamides as a new class of methionine aminopeptidase inhibitors. J Biol Chem **278:** 52964–52971

Turk BE, Griffith EC, Wolf S, Biemann K, Chang YH, Liu JO (1999) Selective inhibition of amino-terminal methionine processing by TNP-470 and ovalicin in endothelial cells. Chem Biol **6:** 823–833

Turk BE, Su Z, Liu JO (1998) Synthetic analogues of TNP-470 and ovalicin reveal a common molecular basis for inhibition of angiogenesis and immunosuppression. Bioorg Med Chem **6:** 1163–1169

Wang J, Lou P, Henkin J (2000) Selective inhibition of endothelial cell proliferation by fumagillin is not due to differential expression of methionine aminopeptidases. J Cell Biochem **77:** 465–473

Weiss LM, Costa SF, Zhang H (2001) Microsporidian methionine aminopeptidase type 2. J Eukaryot Microbiol (Suppl): 88S–90S

Yang G, Kirkpatrick RB, Ho T, Zhang GF, Liang PH, Johanson KO, Casper DJ, Doyle ML, Marino JP Jr, Thompson SK, et al (2001) Steady-state kinetic characterization of substrates and metal-ion specificities of the full-length and N-terminally truncated recombinant human methionine aminopeptidases (type 2). Biochemistry **40:** 10645–10654

Yeh JR, Mohan R, Crews CM (2000) The antiangiogenic agent TNP-470 requires p53 and p21CIP/WAF for endothelial cell growth arrest. Proc Natl Acad Sci USA **97:** 12782–12787

Zhang P, Nicholson DE, Bujnicki JM, Su X, Brendle JJ, Ferdig M, Kyle DE, Milhous WK, Chiang PK (2002) Angiogenesis inhibitors specific for methionine aminopeptidase 2 as drugs for malaria and leishmaniasis. J Biomed Sci **9:** 34–40

Zhang Y, Griffith EC, Sage J, Jacks T, Liu JO (2000) Cell cycle inhibition by the anti-angiogenic agent TNP-470 is mediated by p53 and p21WAF1/CIP1. Proc Natl Acad Sci USA **97:** 6427–6432

Zuo S, Guo Q, Ling C, Chang YH (1995) Evidence that two zinc fingers in the methionine aminopeptidase from *Saccharomyces cerevisiae* are important for normal growth. Mol Gen Genet **246:** 247–253